Energy Advances

ROYAL SOCIETY OF CHEMISTRY

PAPER

View Article Online
View Journal

Cite this: DOI: 10.1039/d6ya00068a

Mechanistic insights into Li_2O_2–solvent reactions: water-induced parasitic chemistry in Li–air batteries

Leonardo H. Baumer, Carmen M. Sinitsyna and Ana E. Torres *

Despite being long considered inert, the common electrolyte solvent acetonitrile can actively participate in parasitic reactions that dictate Li–O_2 battery efficiency. Identifying how solvents interact with discharge products in solution or on the surface is key to mitigating parasitic reactions and extending battery lifetimes. Herein, we present a theoretical mechanistic study on the lithium peroxide degradation products in acetonitrile in the presence of water as a contaminant. Under these conditions, the oxidation of acetonitrile takes place in solution. According to the cluster model, the surface electronic effects are insufficient to initiate the acetonitrile oxidation reaction. Water as a contaminant in Li–O_2/ACN cells participates in LiOH formation that decomposes by reacting with intermediates to produce the original discharge product Li_2O_2, but at the expense of producing the parasitic product acetamide. We proposed a reaction of Li_2O_2 with water to serve as a prototype for conducting intensive and comprehensive computational analysis aimed at testing different solvents for their use in electrolyte solutions or in surface models for Li–O_2 batteries straightforwardly.

Received 6th March 2026,
Accepted 10th March 2026

DOI: 10.1039/d6ya00068a

rsc.li/energy-advances

1. Introduction

Lithium–air batteries promise high energy density and operate through the reduction of O_2 on the surface of a porous carbon-based cathode to form Li_2O_2 during discharge. During charging, the reaction is reversed.[1] The chemistry and performance of the battery depend on the nature of the electrolyte solution, which can affect the oxygen reduction reaction mechanism and may also undergo degradation, so its performance is critically limited by the instability of Li_2O_2 and the parasitic reactions induced by water traces.[2] It has been found that the energy efficiency of the Li–air batteries increases at a specific moisture content. For instance, water addition to aprotic batteries can enhance the first-cycle discharge capacity and lead to a slight increase in the discharge potential.[3,4] However, the lithium anode must be protected in pure air from moisture to prevent corrosion.[5] Therefore, studies on the parasitic chemistry of water in Li–air batteries are needed to understand the causes behind potential benefits and notable limitations.

A critical issue is the degradation of solvents during battery cycling. It has been proposed that Li_2O_2 deposited on the cathode and Li_2O_2 clusters are responsible for such degradation processes. ACN has been identified as an electrolyte solvent with high efficiency in the oxygen reduction/evolution reactions. However, ACN undergoes degradation reactions that have not yet been fully identified. In a practical Li–air battery, an ambient air flow is used, which contains mainly N_2, H_2O, and CO_2. Therefore, studying the influence of water entering with the gas feed is highly relevant, particularly in hygroscopic solvents such as acetonitrile.[6,7] In this context, it has been shown that H_2O induces the formation of soluble lithium hydroperoxide (LiOOH) in the cell, which may increase the capacity but can also lead to the formation of LiOH.[8] These atmospheric contaminants can form antagonistic intermediates and degradation pathways that lead to cell decomposition, which must be identified and eliminated to achieve a practical Li–air battery.[9]

The discharge product, Li_2O_2, is an insulating material with a calculated bandgap greater than 5 eV.[10] This causes overpotential, as there is an increase in the charging potential that contributes to the degradation of both the carbon material in the cathode and the electrolyte. In addition, lithium peroxide can coat the electrode surface, generating electrical resistance, clogging the pores, and preventing oxygen permeation. In this context, it is preferable that Li_2O_2 forms a toroidal morphology rather than a film covering the entire electrode surface. The toroidal morphology of Li_2O_2 leads to a high discharge capacity but a high charge overpotential, whereas the film morphology yields a low overpotential but a low discharge capacity.[11] If this intermediate is adsorbed on the cathode, a film is formed

Micro and Nanotechnologies, Instituto de Ciencias Aplicadas y Tecnología, Universidad Nacional Autónoma de Mexico, CU, Coyoacán, 04510, Mexico City, Mexico. E-mail: ana.torres@icat.unam.mx

through a surface mechanism; if it dissolves in the electrolyte, toroids form through a solution pathway. Therefore, using a solvent that promotes solvation of the intermediates, such as dimethyl sulfoxide, favours the dissolution mechanism and, consequently, the toroidal morphology of Li_2O_2. Li_2O_2 formation *via* a solution mechanism requires the formation of LiO_2 in a solution-intermediate (eqn (1)–(3)) or the dissolution of LiO_2 in a surface-intermediate (eqn (1) and (4));[12] there is no consensus on this point. It is also considered that lithium superoxide is a metastable phase that disproportionates toward Li_2O_2 or can undergo electrochemical reduction to produce the discharge product Li_2O_2. So, LiO_2 is only considered as a reaction intermediate.[13]

$$O_{2(g)} + * + e^- \rightarrow O_2{}^{-}* \quad (1)$$

$$O_2{}^{-}* \rightarrow * + O_{2(sol)}{}^{-} \quad (2)$$

$$2O_{2(sol)}{}^{-} + 2Li^+_{(sol)} \rightarrow 2LiO_{2(sol)} \rightarrow 2Li_2O_2* + O_{2(g)} \quad (3)$$

$$O_2{}^{-}* + Li^+_{(sol)} \rightarrow LiO_2* \rightarrow LiO_{2(sol)} \quad (4)$$

In this sense, the solution-driven discharge product growth requires dissolution of the adsorbed intermediate LiO_2*, thus generating solvated Li^+ and $O_2{}^-$ ions. Such a mechanism is possible in solvents with high Gutmann donor or acceptor numbers. However, $O_2{}^-$ is a strong nucleophile and is known to attack solvents through hydrogen abstraction. However recent contributions highlight the relevance of the $Li^+_{(sol)}O_{2(sol)}{}^-$ association process in solution which is enhanced in low donor number solvents such as acetonitrile, in conjunction with defect-free carbon cathode surfaces that adsorb lithium superoxide weakly.[14]

Alkyl nitriles have been expected to act as stable electrolytes toward Li_2O_2.[15] It has been found theoretically that acetonitrile (ACN) does not undergo degradation on the surface of lithium peroxide under water-free conditions. Instead, ACN interacts strongly with the surface, thus forming a stable interface.[16] Experiments on chemical rechargeability of Li–O_2 batteries by using different solvents have revealed that most rechargeable solvents are ACN and dimethoxyethane (DME). However, none of the electrolytes analyzed exhibited the O_2 recovery efficiency, OER/ORR > 90%, mainly due to secondary oxidative reactions that may occur at high potentials in the charging process.[17]

First-principles-based calculations have shown that the formation of Li_2O_2 from LiO_2 is exothermic in ACN, and Li_2O_2 is thermodynamically more stable than LiO_2. Indeed, it has been found that low potential increases the rate of disproportionation. DFT calculations have shown high reaction energy values for the LiO_2 and ACN reaction (>50 kcal mol^{-1}), thus not being an energetically accessible route for studying.[18] The use of solvents with high donor numbers can contribute to stabilizing $LiO_{2(sol)}$ and Li_2O_2 oxidation at lower potentials, which is not the case herein. The addition of water to an aprotic solvent with a low donor number can aid a solution-mediated mechanism contributing to the reduction of the charge potential and providing improved cyclability. Furthermore, molecular dynamic simulations in ACN have shown a greater solvation energy for Li^+ ions compared to LiO_2, which might indirectly suggest that upon oxygen reduction $Li^+_{(sol)}$–$O_{2(sol)}$ ion pairs are the dominant structures in solution (not $LiO_{2(sol)}$).[19] In addition, the presence of water is expected to enhance the solvation energy of Li^+ far more than that of LiO_2, resulting in preferential Li^+ or Li^+-containing solvated species. Although the formation of ion pairs or LiO_2 is beyond the scope of this work, Li_2O_2 is known to be the dominant discharge product.

Besides the reactions studied herein, it has been reported that $^1O_2$ is responsible also for the parasitic reactions occurring due to cycling of aprotic alkali–metal–oxygen batteries.[20–22] Some experiments have shown that Li_2O_2 forms predominantly *via* solution-mediated disproportionation of superoxide ($O_2{}^-$) in the presence of Li^+ across a wide range of electrolytes and operating conditions, including low-donor-number solvents such as ACN, and remains valid for relatively defect-free carbon-based cathode surfaces, where LiO_2 poorly adsorbs.[23] This disproportionation has been primarily linked to singlet oxygen ($^1O_2$) formation, even at low overpotentials promoted by the presence of protons, as previously reported in the literature.[24,25] However, LiO_2 disproportionation studies on acetonitrile and the singlet oxygen forming mechanisms (as those found for tetraglyme solvent) are limited in the literature and, although they merit further investigation, a comprehensive analysis falls outside the objectives of the present work.

It has been reported that by adding water to an ACN electrolyte, the discharge potential increases and the discharge product corresponds to a mixture of LiOH and Li_2O_2. In this sense, a greater acidity of the aprotic solvent in the presence of traces of water has been found, as indicated by lower pK_a values of water in electrolyte solvents.[26] This leads to stronger solvation of water molecules by the organic solvent that triggers LiOH formation, whereas less acidic solvents produce the reverse effect of weak solvation of water molecules and result in predominant toroidal Li_2O_2 morphologies.[27]

Water molecules can readily interact with nascent Li_2O_2 structures, facilitating solubilization and driving the growth of the structure. For instance, when DME (a solvent in which water has a high pK_a = 47) is used in the electrolyte solution with added water, proton transfer is suppressed.[26,28,29] This reduces the reactivity between superoxide ions and water, thus promoting Li_2O_2 formation on discharge. Then it is expected that a solvent in which water presents a lower pK_a (35.2) such as ACN may promote the formation of LiOH on discharge.[26]

It has been claimed that ACN adsorption on the Li_2O_2 surface activates the sp-hybridized carbon of ACN, facilitating the nucleophilic addition of hydroperoxide in solution to react. After reaction with water, it forms an imidoperoxoic acid intermediate which desorbs from the surface before subsequent reaction with LiOOH in solution to produce acetamide, H_2O and O_2.[9] Two aspects of the proposed mechanism deserve attention. First, while the activation of acetonitrile on the Li_2O_2 surface is suggested to facilitate nucleophilic attack, the precise nature of this activation remains unclear. Second, the mechanism assumes that LiOOH reacts in solution; however, this species may remain bound to Li_2O_2 particles or the surface,

which could substantially influence the reaction pathway. Herein, these points are addressed in the present study to clarify the roles of solvent effects and surface interactions, considered within the framework of a cluster model.

We studied H_2O-mediated degradation mechanisms in solution for Li–O_2 cells containing an ACN-based electrolyte and performed a comparative analysis of the initial degradation step with other solvents such as dimethylacetamide (DMA), dimethyl sulfoxide (DMSO), triethylamine (TEA) and dimethylformamide (DMF). Through *ab initio* calculations, we revealed mechanistic differences between cluster and molecular Li_2O_2 pathways in aprotic solvents, uncovering how water alters decomposition and drives side reactions. These insights provide guidelines for solvent selection and electrolyte design, bridging microscopic chemistry with practical battery performance.

2. Computational details

The chemical species involved in the degradation pathway of the acetonitrile molecule in the presence of water were modeled using density functional theory (DFT) with the Gaussian 16 software, both in a vacuum and employing an implicit solvent model (SMD).[30–32] The geometries of the reactant and product molecules were optimized and characterized as energy minimum or transition-state structures through vibrational frequency analysis. The M06-2X functional[33] and the 6-31+G(d,p) basis set were used.[34] The energies of each chemical species involved in the reaction were calculated, and the reaction energies were computed by referring to the reactants. The reaction free energies and free activation energies were computed for the Li_2O_2 and water reaction in the different solvents at 25 °C. This methodology is widely used to assess free energy and reaction pathways involved in processes within lithium–air batteries under ambient operating conditions and provides a reliable description of the underlying potential energy surface.[35–37] The nature of the stationary points along the potential energy surface was confirmed as energy minima or transition structures through vibrational frequency calculations. The connectivity between reactants, products and the transition structures was verified through the intrinsic reaction coordinate (IRC). Generalized atomic polar tensor-derived charges were computed for optimized structures.[38] The calculations were performed using Gaussian 16 software.[39]

A molecular and cluster-based modeling framework was adopted to investigate the Li_2O_2 reaction with acetonitrile in the presence of water. In this context, the particle-based models have shown their utility in describing Li_2O_2 formation, as finite Li_2O_2 clusters can reasonably represent the nascent discharge product structures formed during Li–O_2 battery operation.[40–43] Such clusters expose a diversity of reactive sites, including peroxo, superoxo, and Li–O–Li moieties, which may better reflect the structural heterogeneity expected in freshly formed discharge products. Experimentally, in the presence of trace amounts of water when ACN is used as the electrolytic solvent, small Li_2O_2 toroidal particles as well as LiOH flower-like structures have been observed.[26] These morphologies indicate that the discharge products formed under realistic operating conditions do not necessarily correspond to well-defined crystalline surfaces, but instead exhibit nanoscale dimensions, curvature, and likely defect-rich or heterogeneous structural features. Although some reported Li_2O_2 toroids are described as highly crystalline, with the (001) facet oriented normal to the toroid axis, their overall morphology remains nanoscale and curved rather than planar and extended.[44] Accordingly, the molecular and cluster model adopted here is intended to capture the structural and electronic characteristics of localized coordination environments that are likely to govern interfacial chemical reactivity at nascent discharge products.

3. Results and discussion

3.1. Li_2O_2 reactions with acetonitrile in the presence of water

First, the discharge product Li_2O_2 in acetonitrile must react with water or interact with CH_3CN. By comparing these molecular interactions energetically, within the continuum solvent model, their computed binding energies are -22 kcal mol^{-1} for Li_2O_2–H_2O *vs.* -12.4 kcal mol^{-1} for Li_2O_2–CH_3CN, which demonstrate a preferential interaction of water with lithium peroxide. Then, it must react with the partner molecule to form LiOH and LiOOH and afterwards interact with acetonitrile. The binding energy of the LiOOH–LiOH intermediate with CH_3CN is -13.2 kcal mol^{-1}, which exceeds that of this intermediate but embedded in a cluster model (-12.4 kcal mol^{-1}) representing a Li_2O_2 solid nascent structure. The dipole-derived atomic charges obtained from the atomic polar tensor, shown in Fig. 1, have shown meaningless changes on charges for the C$\equiv$N moiety with the binding of acetonitrile to Li_2O_2, to the hydroxylated lithium peroxide molecule or to the hydroxylated $(Li_2O_2)_4$ cluster. Within the molecular and cluster models used in the present work, no meaningful C–N bond distances elongation on ACN were detected suggesting bond activation, thus ruling out an induced charge polarization in the nitrile bond through Li_2O_2 interaction. This finding may apply to localized Li–O moieties considered in the present model; the potential influence of long-range polarization effects on an extended lithium peroxide surface remains to be determined. To assess whether Li_2O_2 hydroxylation is preferred in solution or on the surface, we study the reaction pathway leading to LiOOH and LiOH products as shown in Scheme 1 and Fig. 2.

In a molecular approach, this reaction is exothermic by -13.2 kcal mol^{-1}, comparable to the stability determined in the DME solvent,[46] with a surmountable barrier height of 2.6 kcal mol^{-1}. In a $(Li_2O_2)_4$ cluster model, this barrier has a similar value (2.8 kcal mol^{-1}), leading to a product exhibiting nearly the same stability (-16 kcal mol^{-1}). The optimized cluster structures are presented in Fig. 3. In comparison, this reaction proceeds through an almost barrierless pathway in the DME solvent, as studied by us previously.[45]

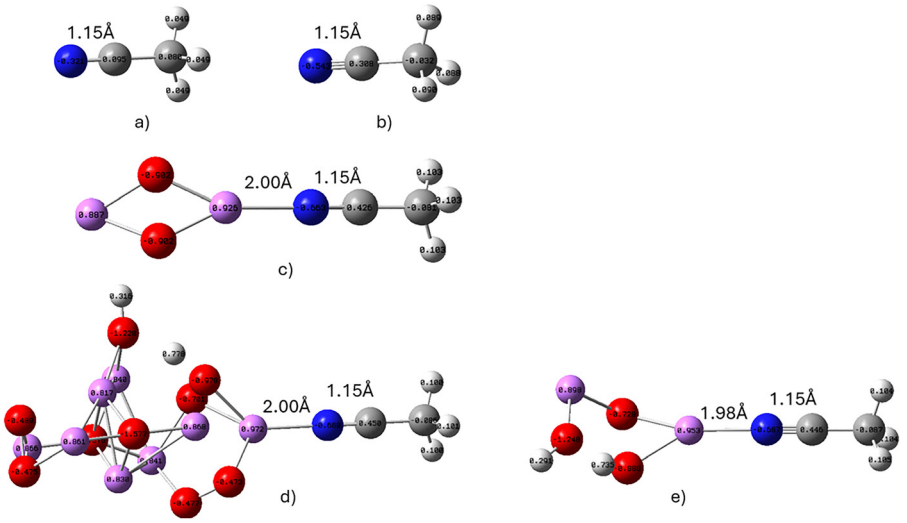

Fig. 1 Dipole-derived atomic charges obtained from the Atomic Polar Tensor for ACN in vacuum (a), and the following species under continuum solvent model (acetonitrile) (b), Li_2O_2-ACN (c), hydroxylated $(Li_2O_2)_4$ cluster-ACN (d), and hydroxylated lithium peroxide molecule-ACN (e). Color code: C: grey, N: blue, H: white, O: red and Li: pink.

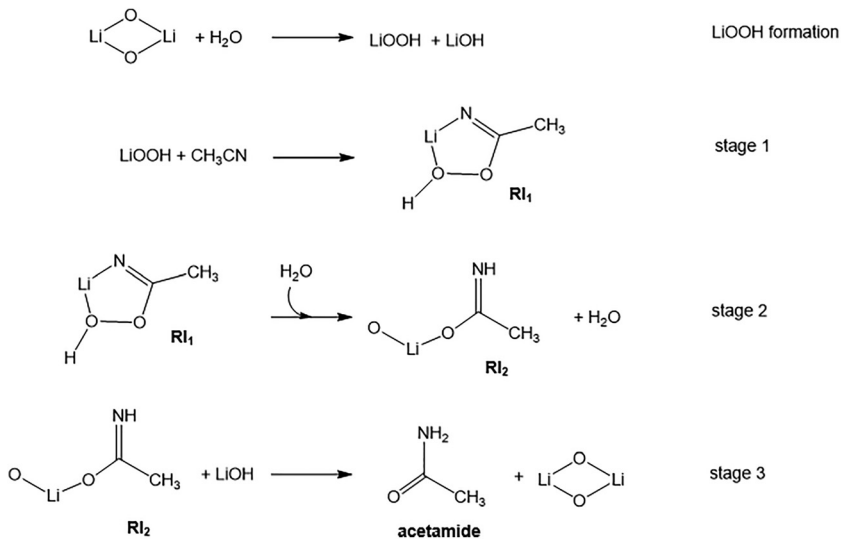

Scheme 1 Reactions of the discharge product Li_2O_2 with water and acetonitrile.

These results show that the formation of LiOH and LiOOH is energetically viable at the molecular level in solution or within a lithium peroxide nascent solid structure in the presence of a water molecule contaminant. The last step in the reaction pathway corresponds to the dissociation energy of the adduct, which is required to perform further calculations; this step does not exhibit a reaction barrier. Some of the reaction pathways displayed in the present work show blue dotted lines that connect each electrostatic minimum with the separated fragments. Due to the electrostatic nature of the species formed, the products remain interacting through Coulombic forces and must be separated to enable subsequent chemical reactions, as discussed in a previous contribution.[46]

Because of the very electropositive nature of the alkali metals, the known solid alkali lithium oxides (LiO_2 and Li_2O_2) can hydrolyze in water to produce LiOH and in some cases H_2O_2. Spectrometric determinations in model Li–O_2 cells revealed the complete hydrolysis of LiO_2 to LiOH,[47] whereas theoretical calculations in vacuum as reported in ref. 42 indicate that Li_2O_2 hydrolysis leading to LiOH and H_2O_2 formation is highly endothermic, while the direct conversion to LiOH that avoids H_2O_2 production is exothermic. Moreover, when water molecules were included in the solvation shell, the hydrolysis of Li_2O_2 leading to H_2O_2 formation exhibited a slightly exothermic character (-2 kcal mol^{-1}) as previously reported,[47] which does not compete with the reaction pathway of Li_2O_2 and water

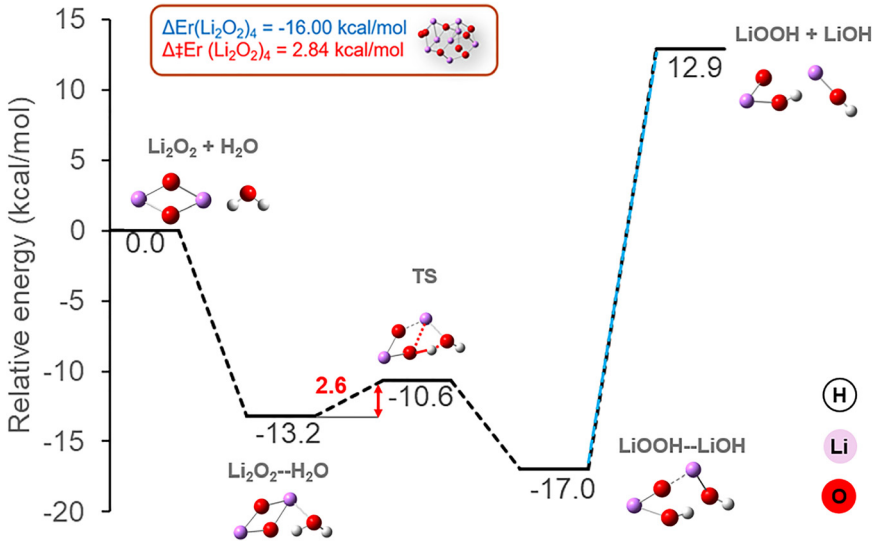

Fig. 2 LiOH and LiOOH formation reaction pathway.

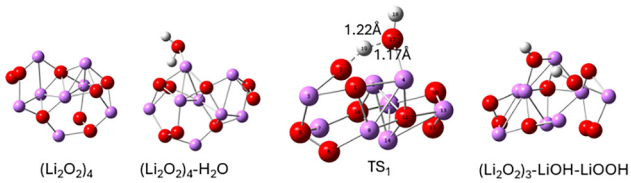

Fig. 3 Optimized Li_2O_2 tetramer within the continuum solvent model (ACN) and its corresponding hydroxylated products after water addition. The $(Li_2O_2)_4$ cluster structure is taken from our previous contribution.[45] The transition structure is presented (TS_1) along with relevant bond distances.

molecule leading to LiOOH formation, shown in Fig. 2, which is substantially more exothermic (−17 kcal mol^{-1}). For this reason, the hydrolysis pathway involving H_2O_2 formation was not considered further in this work.

The mechanism of the uncatalyzed partial hydrolysis of acetonitrile to acetamide has been described as a three-step sequence involving: (i) nucleophilic addition of water to the nitrile carbon, (ii) isomerization of the hydroxy imine intermediate, and (iii) tautomerization leading to amide formation.[48]

Then, the first stage of the reaction proceeds with LiOOH and ACN interaction, reacting to form a C–O bond by surmounting an energy barrier of 15.9 kcal mol^{-1}, leading to a 5-ring-membered intermediate RI_1 displayed in Fig. 4, with a stability comparable to that of the reactants. LiOOH attack is studied over cyanide carbon of acetonitrile since, even in the

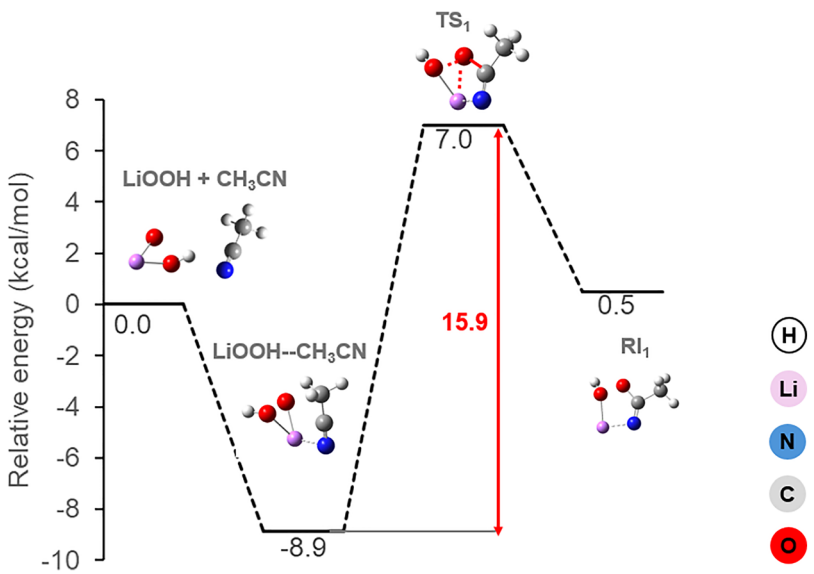

Fig. 4 First reaction stage: LiOOH reaction with ACN.

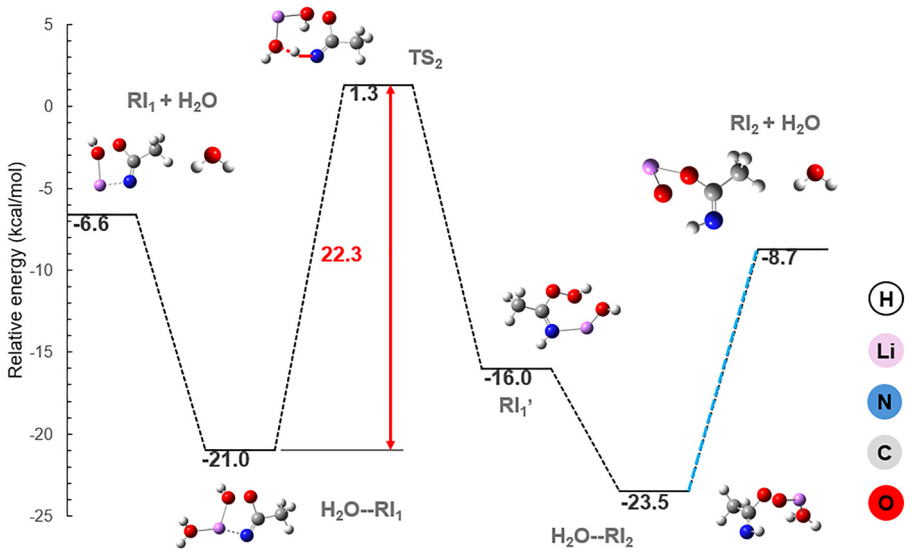

Fig. 5 Second stage: LiOOH reaction with ACN.

absence of water, superoxide addition is preferred in this site, but with an energy barrier higher than that computed in Fig. 4 (23.7–24.9 kcal mol^{-1}) and through an endothermic reaction pathway.[49]

Comparatively, direct oxidation of acetonitrile by Li_2O_2 molecule in vacuum is prohibitive due to a high energy barrier of 254.6 kcal mol^{-1} computed at the B3LYP/6-311G level of theory.[18]

The second stage of the reaction (Fig. 5) is assisted by the addition of a second water molecule interacting with the RI_1 intermediate in which the imine abstracts the first hydrogen from H_2O. This process occurs through a higher barrier of 22.3 kcal mol^{-1}, leading to a reactive intermediate RI_1' which evolves without an energy barrier to the H_2O–RI_2 product (Fig. 5). This RI_1' intermediate forms through intramolecular tautomerization, so the hydrogen for imine formation comes from added water and then a proton from the OOH moiety migrates to the OH fragment to regenerate a water molecule. Then, as shown in Fig. 5 water must be desorbed from RI_2 for further reaction.

In the third stage, shown in Fig. 6, since LiOH has already been produced in stage 1, it is added to interact with species RI_2 so that a second hydrogen abstraction might take place, leading to acetamide and Li_2O_2 production with an energy barrier of 32.7 kcal mol^{-1}. Li_2O_2 may oxidize towards the molecular oxygen evolution in the following cycling process.

The third stage corresponds to the limiting step in this chemical transformation to produce acetamide. Experiments

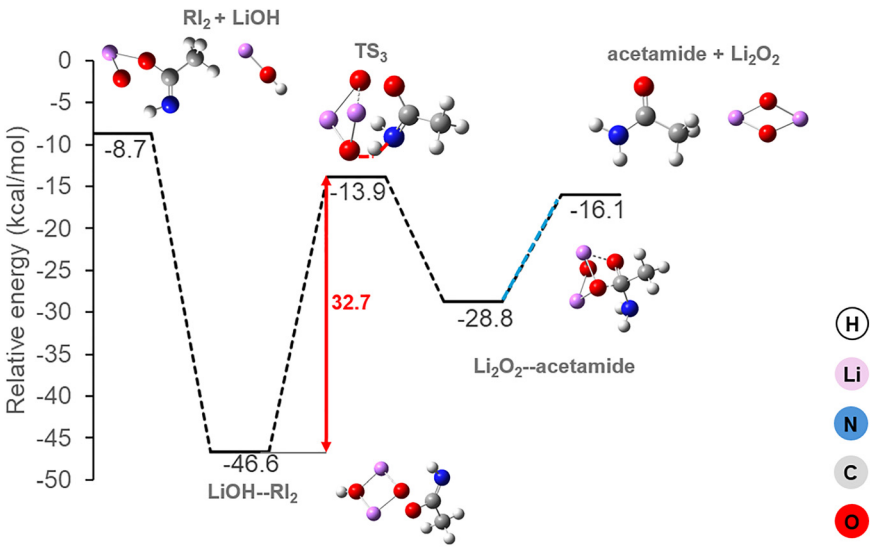

Fig. 6 LiOOH reaction with ACN, third stage toward acetamide formation.

Table 1 Reaction energies (ΔE) and Gibbs free energies (ΔG) in kcal mol^{-1}

Reaction	ΔE	ΔG
LiOOH formation	12.9	11.4
Stage 1	0.5	13.7
Stage 2	−2.0	−2.9
Stage 3	−7.4	−8.0

have shown that in the presence of OH^-, the superoxide ion reacts with acetonitrile to produce acetamide in small yields, which is consistent with the third stage of the reaction.[50,51] The computed reaction energies and Gibbs free energies for each stage in the transformation from acetonitrile to acetamide are summarized in Table 1.

In the present work, the computed Gibbs free energy change for the reaction $H_2O + CH_3CN \rightarrow CH_3CONH_2$ is −8.6 kcal mol^{-1}, in reasonable agreement with the reported value of −11.2 kcal mol^{-1} computed in vacuum.[48] Despite its thermodynamic feasibility, the reaction is kinetically constrained. Literature reports indicate that the rate-determining step, corresponding to the nucleophilic addition of water to acetonitrile, proceeds through an activation barrier exceeding 64 kcal mol^{-1}.[48] Such a substantial barrier hinders the uncatalyzed hydrolysis under ambient conditions, highlighting the dominant role of kinetic constraints over thermodynamic driving force in this reaction.

It is known that nitriles can be converted into amides by heating them in a weakly basic medium in the presence of hydrogen peroxide.[52] NAP-XPS characterization using a solid–electrolyte model cell has shown that acetonitrile is chemically unstable in the presence of Li–O_2 discharge products, including Li_2O_2, undergoing oxidation during and after discharge. While this aspect was not discussed in the article, the electrolyte employed was acetonitrile, which may contain trace amounts of water. The authors reported the use of acetonitrile (anhydrous, 99.8%, Sigma-Aldrich), corresponding to a specified H_2O content of <10–50 ppm.[18] In another study, the stability of Li–O_2 cells employing a MeCN-based electrolyte was investigated using model systems. Analysis of the cycled electrolyte identified acetamide as the major degradation product under both cell and model conditions. Experiments used dried acetonitrile (99.999%, Aldrich; ∼4 ppm H_2O), while Karl Fischer titration of electrolyte extracted from assembled cells indicated an increased water content of ≈150 ppm, maybe due to handling and cell assembly. [9]Finally, related evidence for acetonitrile hydrolysis has emerged from electrochemical studies aimed at amide synthesis *via* oxygen activation. Results revealed that the electrocatalytic pathway that undergoes through –O_2– or –OOH intermediates is essential for steering acetonitrile toward acetamide production. Imine peroxyl intermediate (R–C(O–O–)═NH) is determined as a key intermediate through *in situ* FTIR analysis.[53]

Acetonitrile (MeCN) is a suitable solvent for nonaqueous electrolytes tolerant toward oxidation. However, it is unstable in reductive media such as the lithium metal anode. As a reducing agent, Li metal induces reduction and decomposition of acetonitrile, hindering the formation of a stable SEI. Some strategies have been used to overcome solvent drawbacks, explained as follows. For instance, the use of high-concentration ACN-based electrolytes introduces more anions that solvate Li ions, preventing solvent reactivity.[54–56] However, this comes at the expense of increased viscosity and higher electrolyte salt costs. Alternatively, additives for solid electrolyte interface (SEI) formation have been used in electrolytic solutions to suppress solvent decomposition. Also, the chemical pretreatment of lithium metal with some additives creates an effective passivation layer against ACN reduction.[57] Nevertheless, these strategies have been mainly explored in lithium-ion battery systems[58] and not in lithium–air batteries. Thus, leaving open significant opportunities for improvement on the anode side.

3.2. Li_2O_2 reactions with the water molecule in aprotic solvents

For comparison, the reaction of Li_2O_2 with water (see Fig. 2) is studied as a prototype reaction to compare the susceptibility of each solvent to form LiOH and LiOOH parasitic products. Then, the reaction pathway as presented in Fig. 2 is studied in different solvents: dimethylformamide (DMF), dimethylacetamide (DMA), dimethylsulfoxide (DMSO), triethylamine (TEA), dimethoxyethane (DME) and acetonitrile (ACN), using an SMD continuum solvent model. The Gibbs free reaction energies at 25 °C and their corresponding Gibbs free activation energies are presented in Table 2.

According to computed results, DMF and DME present low free energy reaction barriers at 25 °C to form hydroxylation products, whereas ACN presents a higher energy barrier that may be achievable on cycling. Interestingly, even though TEA has the greatest Gutmann donor number, the reaction free energy barrier and reaction free energy do not follow the expected trend of the lowest values among the analyzed solvents. The available computed pK_a values of water in each solvent (ACN = 35.2, DMF = 43.4, DME < 47 and DMA = 45.7) do not explain by themselves the greater stability of nitrile solvents during discharge.[26] Nevertheless, when analyzed in conjunction with the data displayed in Table 2, they may provide a useful descriptor of parasitic behaviour in Li–air chemical environments. Overall, the computed Gibbs free activation energies indicate that the required energy barriers are accessible under typical battery operating conditions. Then, in the presence of water, even if the solvents present a low

Table 2 Gibbs free reaction energy (ΔG_r), Gibbs free activation energy ($\Delta G^{\ddagger}$) of LiOH formation in different solvents and their Gutman donor number values (DN)

Solvent	DMF	DMA	DMSO	DME	TEA	ACN
ΔG_r (kcal mol^{-1}) 25 °C	−2.45	−2.42	−1.54	−2.60	−2.19	−1.03
$\Delta G^{\ddagger}$ (kcal mol^{-1}) 25 °C	0.24	0.27	1.16	0.16	0.72	1.88
DN[a]	26.6	27.8	29.8	24	61	14.1

[a] Taken from ref. 59.

donor number, parasitic reactions between the discharge product and water may occur and trigger solvent decomposition.

These results deserve further discussion since previous studies reported that direct decomposition of Li_2O_2 with H_2O corresponds to an endergonic reaction requiring a Gibbs free energy of 9.8 kcal mol^{-1} to form LiOH and H_2O_2, computed from Gibbs free energy of formation values.[4] Then, the reaction energy barrier should exceed this theoretical value.

To better understand the possible sources of protons in the system, the electrooxidation of water requires an applied potential of 3.7 V *vs.* Li/Li^+ to produce H^+.[4] However, in a recent study, the estimated discharge potential remained below this value (2.7 eV), so protons may not originate from direct water electroreduction during discharge.[9] Indeed, by using DME, Li_2O_2 is only reported as the discharge product even in the presence of water.[4] During cycling, H_2O_2 is likely generated at elevated charging potentials, where the formation of H^+ enables subsequent reaction with Li_2O_2 to produce hydrogen peroxide and Li^+.[26] However, in the presence of water, the nucleophilic $LiOO^-$ species within Li_2O_2 are expected to react preferentially with the available protons from water, leading to the formation of a LiOH–LiOOH intermediate as revealed through previous computational studies.[45,46] Even during discharge, if H_2O_2 is formed, as reported in previous studies,[60] its subsequent interaction with the LiOH discharge product would lead to the formation of the same intermediate species LiOOH–LiOH that ultimately will evolve to the Li_2O_2–H_2O adduct through an energetically favorable exothermic pathway as reported in ref. 46. Increasing water content favors the formation of H_2O_2 and LiOH during discharge, leading to higher concentrations of the LiOOH–LiOH intermediate and, consequently, more Li_2O_2 and H_2O. At minimum potentials of 2.96V, Li_2O_2 is oxidized, leading to the regeneration of Li and O_2 during charging.

Revisiting the decomposition of lithium oxide, the reaction pathway proposed in this study offers an alternative route that directly connects to acetamide formation on discharge, bypassing hydrogen evolution *via* electrolytic reactions and revealing chemical pathways that may occur in nitrile solvents in the presence of water.

4. Conclusions

In the presence of water, it is found that acetonitrile may oxidize to carboxamides. The interaction of Li_2O_2 with ACN produces weakly adsorbed species, which is the case, as found from computed binding energies between Li_2O_2 and ACN with values near 0.5 eV, indicative of physisorption. Indeed, results have shown that the oxidation of acetonitrile takes place with lithium peroxide in solution. The surface effect, within a cluster model approach, does not appear to be sufficiently significant to enable the occurrence of the reaction. From the theoretical results, the interactions on the surface of a cluster model and in the ACN solution are of the same electrostatic nature. Water as a contaminant in Li–O_2/ACN cells participates in LiOH formation, and this product might influence the reactive media to facilitate ACN oxidation. A positive point is that even if LiOH is produced it will further decompose by reacting with the ACN–LiOOH intermediate to produce the original discharge product Li_2O_2, but at the expense of the parasitic product acetamide, which will decrease the cell efficiency. We consider the Li_2O_2 and water reaction to serve as a prototype for conducting intensive and comprehensive analysis aimed at testing different solvents for use in electrolyte solutions of this type of battery. We emphasize this point since this reaction inherently includes information on the acidity of water in that medium and describes the propensity for parasitic reactions which can be screened in solution or in surface models straightforwardly.

This study establishes a mechanistic foundation for understanding chemical reactivity at the interphase between the electrolyte and the nascent Li_2O_2 discharge product structures. By identifying reaction pathways and key intermediates, our results provide fundamental insight into the factors controlling Li–O_2 battery stability. These findings lay the groundwork for future dynamic simulations aimed at capturing the evolution of the cathode interface under realistic operating conditions.

Author contributions

The manuscript was written through contributions of all authors. All authors have given approval to the final version of the manuscript. L. H. Baumer and C. M. Sinitsyna contributed equally to the computational calculations and data analysis, and share first authorship. A. E. Torres supervised the work, guided the project and edited the manuscript.

Conflicts of interest

There are no conflicts to declare.

Data availability

The data supporting this article have been included as part of the supplementary information (SI). Supplementary information: coordinates of the optimized geometries for stationary points found along the reaction pathway. See DOI: https://doi.org/10.1039/d6ya00068a.

Acknowledgements

The authors gratefully acknowledge DGTIC-UNAM for the use of supercomputer facilities through the project LANCAD-UNAM- DGTIC-401 and Centro Nacional de Supercómputo del IPICyT, A. C., through the project TKII-E-0523-I-110523-9 that have contributed to the research results reported within this paper. A. E. T. acknowledges financial support provided by the DGAPA-PAPIIT IN218825 grant.

Notes and references

1 M. C. Policano, C. G. Anchieta, T. C. M. Nepel, R. M. Filho and G. Doubek, *ACS Appl. Energy Mater.*, 2022, **5**, 9228–9240.

2 T. Liu, J. P. Vivek, E. W. Zhao, J. Lei, N. Garcia-Araez and C. P. Grey, *Chem. Rev.*, 2020, **120**, 6558–6625.
3 Y. G. Zhu, Q. Liu, Y. Rong, H. Chen, J. Yang, C. Jia, L.-J. Yu, A. Karton, Y. Ren, X. Xu, S. Adams and Q. Wang, *Nat. Commun.*, 2017, **8**, 14308.
4 K. U. Schwenke, M. Metzger, T. Restle, M. Piana and H. A. Gasteiger, *J. Electrochem. Soc.*, 2015, **162**, A573.
5 G. Wang, L. Huang, S. Liu, J. Xie, S. Zhang, P. Zhu, G. Cao and X. Zhao, *ACS Appl. Mater. Interfaces*, 2015, **7**, 23876–23884.
6 Z. Liang, W. Wang and Y.-C. Lu, *Joule*, 2022, **6**, 2458–2473.
7 S. Wagenfeld, W. Schröer and B. Rathke, *J. Chem. Eng. Data*, 2024, **69**, 2273–2292.
8 M. Tułodziecki, G. M. Leverick, C. V. Amanchukwu, Y. Katayama, D. G. Kwabi, F. Bardé, P. T. Hammond and Y. Shao-Horn, *Energy Environ. Sci.*, 2017, **10**, 1828–1842.
9 R. C. McNulty, K. D. Jones, C. Holc, J. W. Jordan, P. G. Bruce, D. A. Walsh, G. N. Newton, H. W. Lam and L. R. Johnson, *Adv. Energy Mater.*, 2023, **13**, 2300579.
10 M. D. Radin, F. Tian and D. J. Siegel, *J. Mater. Sci.*, 2012, **47**, 7564–7570.
11 B. D. Adams, C. Radtke, R. Black, M. L. Trudeau, K. Zaghib and L. F. Nazar, *Energy Environ. Sci.*, 2013, **6**, 1772–1778.
12 Y. Wang and Y.-C. Lu, *Energy Storage Mater.*, 2020, **28**, 235–246.
13 A. Y. Tesio, W. Torres, M. Villalba, F. Davia, M. del Pozo, D. Córdoba, F. J. Williams and E. J. Calvo, *ChemElectroChem*, 2022, **9**, e202201037.
14 C. Prehal, S. Mondal, L. Lovicar and S. A. Freunberger, *ACS Energy Lett.*, 2022, **7**, 3112–3119.
15 R. Younesi, P. Norby and T. Vegge, *ECS Electrochem. Lett.*, 2014, **3**, A15.
16 B. D. McCloskey, D. S. Bethune, R. M. Shelby, T. Mori, R. Scheffler, A. Speidel, M. Sherwood and A. C. Luntz, *J. Phys. Chem. Lett.*, 2012, **3**, 3043–3047.
17 G. Leverick, M. Tułodziecki, R. Tatara, F. Bardé and Y. Shao-Horn, *Joule*, 2019, **3**, 1106–1126.
18 T. K. Zakharchenko, A. I. Belova, A. S. Frolov, O. O. Kapitanova, J.-J. Velasco-Velez, A. Knop-Gericke, D. Vyalikh, D. M. Itkis and L. V. Yashina, *Top. Catal.*, 2018, **61**, 2114–2122.
19 B. R. Didar and A. Groß, *Chin. J. Catal.*, 2022, **43**, 2850–2857.
20 N. Mahne, O. Fontaine, M. O. Thotiyl, M. Wilkening and S. A. Freunberger, *Chem. Sci.*, 2017, **8**, 6716–6729.
21 D. Córdoba, L. N. Benavides, D. H. Murgida, H. B. Rodríguez and E. J. Calvo, *Faraday Discuss.*, 2024, **248**, 190–209.
22 W.-J. Kwak, H. Kim, Y. K. Petit, C. Leypold, T. T. Nguyen, N. Mahne, P. Redfern, L. A. Curtiss, H.-G. Jung, S. M. Borisov, S. A. Freunberger and Y.-K. Sun, *Nat. Commun.*, 2019, **10**, 1380.
23 C. Prehal, S. Mondal, L. Lovicar and S. A. Freunberger, *ACS Energy Lett.*, 2022, **7**, 3112–3119.
24 A. P. Gualdron-Plata, V. Y. Brizola and V. L. Martins, *ChemElectroChem*, 2025, **12**, e202500051.
25 A. Pierini, S. Brutti and E. Bodo, *ChemPhysChem*, 2020, **21**, 2060–2067.
26 D. G. Kwabi, T. P. Batcho, S. Feng, L. Giordano, C. V. Thompson and Y. Shao-Horn, *Phys. Chem. Chem. Phys.*, 2016, **18**, 24944–24953.
27 T. Laino and A. Curioni, *New J. Phys.*, 2013, **15**, 95009.
28 Q. Dong, X. Yao, Y. Zhao, M. Qi, X. Zhang, H. Sun, Y. He and D. Wang, *Chemistry*, 2018, **4**, 1345–1358.
29 A. Khetan, A. Luntz and V. Viswanathan, *J. Phys. Chem. Lett.*, 2015, **6**, 1254–1259.
30 A. V. Marenich, C. J. Cramer and D. G. Truhlar, *J. Phys. Chem. B*, 2009, **113**, 6378–6396.
31 R. F. Ribeiro, A. V. Marenich, C. J. Cramer and D. G. Truhlar, *J. Phys. Chem. B*, 2011, **115**, 14556–14562.
32 J. Ho and M. Z. Ertem, *J. Phys. Chem. B*, 2016, **120**, 1319–1329.
33 Y. Zhao and D. G. Truhlar, *Theor. Chem. Acc.*, 2008, **120**, 215–241.
34 R. Ditchfield, W. J. Hehre and J. A. Pople, *J. Chem. Phys.*, 1971, **54**, 724–728.
35 W. Fan, X. Liu, G. Li, K. Yu, P. Wang, M. Lei, C. Zhen, L. Miao, J. Wang, C. Li, J. Hou, H. Ji and L. Miao, *Batteries*, 2025, **11**, 349.
36 B. B. Behera and B. S. Mallik, *Comput. Theor. Chem.*, 2025, **1254**, 115539.
37 A. Pierini, A. Petrongari, V. Piacentini, S. Brutti and E. Bodo, *J. Phys. Chem. A*, 2023, **127**, 9229–9235.
38 W. E. Richter, L. J. Duarte and R. E. Bruns, *J. Chem. Inf. Model.*, 2021, **61**, 3881–3890.
39 M. J. Frisch, G. W. Trucks, H. B. Schlegel, G. E. Scuseria, M. A. Robb, J. R. Cheeseman, G. Scalmani, V. Barone, G. A. Petersson, H. Nakatsuji, X. Li, M. Caricato, A. V. Marenich, J. Bloino, B. G. Janesko, R. Gomperts, B. Mennucci, H. P. Hratchian, J. V. Ortiz, A. F. Izmaylov, J. L. Sonnenberg, D. Williams-Young, F. Ding, F. Lipparini, F. Egidi, J. Goings, B. Peng, A. Petrone, T. Henderson, D. Ranasinghe, V. G. Zakrzewski, J. Gao, N. Rega, G. Zheng, W. Liang, M. Hada, M. Ehara, K. Toyota, R. Fukuda, J. Hasegawa, M. Ishida, T. Nakajima, Y. Honda, O. Kitao, H. Nakai, T. Vreven, K. Throssell, J. A. Montgomery Jr., J. E. Peralta, F. Ogliaro, M. J. Bearpark, J. J. Heyd, E. N. Brothers, K. N. Kudin, V. N. Staroverov, T. A. Keith, R. Kobayashi, J. Normand, K. Raghavachari, A. P. Rendell, J. C. Burant, S. S. Iyengar, J. Tomasi, M. Cossi, J. M. Millam, M. Klene, C. Adamo, R. Cammi, J. W. Ochterski, R. L. Martin, K. Morokuma, O. Farkas, J. B. Foresman and D. J. Fox, 2016, preprint.
40 M. K. Alam, S. Emon and H. Takaba, *Phys. Chem. Res.*, 2025, **13**, 677–686.
41 Z. Gan, X. Lei, B. Hou, M. Luo, S. Zhong and C. Ouyang, *J. Cluster Sci.*, 2020, **31**, 643–649.
42 K. C. Lau, R. S. Assary, P. Redfern, J. Greeley and L. A. Curtiss, *J. Phys. Chem. C*, 2012, **116**, 23890–23896.
43 R. S. Assary, K. C. Lau, K. Amine, Y.-K. Sun and L. A. Curtiss, *J. Phys. Chem. C*, 2013, **117**, 8041–8049.
44 Z. Lyu, Y. Zhou, W. Dai, X. Cui, M. Lai, L. Wang, F. Huo, W. Huang, Z. Hu and W. Chen, *Chem. Soc. Rev.*, 2017, **46**, 6046–6072.
45 A. E. Torres, E. Ramos and P. B. Balbuena, *J. Phys. Chem. C*, 2020, **124**, 10280–10287.

46 A. E. Torres and P. B. Balbuena, *Chem. Mater.*, 2018, **30**, 708–717.
47 H.-H. Wang, Y. J. Lee, R. S. Assary, C. Zhang, X. Luo, P. C. Redfern, J. Lu, Y. J. Lee, D. H. Kim, T.-G. Kang, E. Indacochea, K. C. Lau, K. Amine and L. A. Curtiss, *J. Phys. Chem. C*, 2017, **121**, 9657–9661.
48 J. Ma, X. Zhang, N. Zhao, F. Xiao, W. Wei and Y. Sun, *J. Mol. Struct. THEOCHEM*, 2009, **911**, 40–45.
49 V. S. Bryantsev, V. Giordani, W. Walker, M. Blanco, S. Zecevic, K. Sasaki, J. Uddin, D. Addison and G. V. Chase, *J. Phys. Chem. A*, 2011, **115**, 12399–12409.
50 K. Yamaguchi, T. S. Calderwood and D. T. Sawyer, *Inorg. Chem.*, 1986, **25**, 1289–1290.
51 Y. Sawaki and Y. Ogata, *Bull. Chem. Soc. Jpn.*, 1981, **54**, 793–799.
52 J. H. Hall and M. Gisler, *J. Org. Chem.*, 1976, **41**, 3769–3770.
53 L.-Y. Dong, Y.-T. Wu, Y.-F. Wang, M.-Y. Zhu, H. Wang, G.-P. Hao and A.-H. Lu, *Angew. Chem., Int. Ed.*, 2025, **64**, e202513359.
54 W. Zhang, H. Sun, P. Hu, W. Huang and Q. Zhang, *EcoMat*, 2021, **3**, e12128.
55 Y. Yamada, K. Furukawa, K. Sodeyama, K. Kikuchi, M. Yaegashi, Y. Tateyama and A. Yamada, *J. Am. Chem. Soc.*, 2014, **136**, 5039–5046.
56 M. Li, Y. Liu, X. Yang, Q. Zhang, Y. Cheng, L. Deng, Q. Zhou, T. Cheng and M. D. Gu, *Adv. Mater.*, 2024, **36**, 2404271.
57 N. D. Trinh, D. Lepage, D. Aymé-Perrot, A. Badia, M. Dollé and D. Rochefort, *Angew. Chem.*, 2018, **130**, 5166–5169.
58 H. Du, Y. Wang, Y. Kang, Y. Zhao, Y. Tian, X. Wang, Y. Tan, Z. Liang, J. Wozny, T. Li, D. Ren, L. Wang, X. He, P. Xiao, E. Mao, N. Tavajohi, F. Kang and B. Li, *Adv. Mater.*, 2024, **36**, 2401482.
59 V. Gutmann, *Electrochim. Acta*, 1976, **21**, 661–670.
60 H.-H. Wang, Y. J. Lee, R. S. Assary, C. Zhang, X. Luo, P. C. Redfern, J. Lu, Y. J. Lee, D. H. Kim, T.-G. Kang, E. Indacochea, K. C. Lau, K. Amine and L. A. Curtiss, *J. Phys. Chem. C*, 2017, **121**, 9657–9661.